Indian Journal of Chemical Technology
Vol. 32, May 2025, pp. 355-366
DOI: 10.56042/ijct.v32i3.13964

Enhancing the structural and morphological properties of cerium oxide nanostructures for effective corrosion protection of mild steel

A. Sivasubramanian[1]* & R. Maheswaran[2]

[1]Department of Mechanical Engineering, VV College of Engineering, Tisaiyanvilai, Tamil Nadu, India

[2]Department of Mechanical Engineering, Mepco Schlenk Engineering College (Autonomous), Sivakasi, Tamil Nadu, India

*E-mail: ssgokul81@gmail.com

Received 25 September 2024; accepted 13 January 2025

The widespread issue of metal corrosion, particularly in harsh environments such as acidic, alkaline, and saline conditions, poses significant challenges to the durability and functionality of materials. Cerium oxide nanoparticles (CeO_2 NPs) have been prepared in this study using a sonication-assisted green synthesis technique with the extract of *Nelumbo nucifera* leaves serving as a reducing and stabilizing agent. Comprehensive characterization techniques, including XRD, FESEM, HRTEM and DLS are used to investigate the structural phase, crystalline properties, and morphology of the synthesized nanoparticles. The optical properties are analyzed using UV–visible and photoluminescence (PL) spectroscopy, while FTIR identified the functional groups responsible for stabilization. The EIS and potentiodynamic polarization techniques are utilized to evaluate the corrosion behaviour of CeO_2-coated mild steel (MS) plates compared to uncoated MS plates in various electrolytes: 1M HCl, 1M KOH, and 3.5% NaCl. The Nyquist plot revealed the conducting nature of the material, forming a characteristic semicircle indicative of charge transfer resistance. The Tafel plot provided insights into the corrosion activity of coated and uncoated MS plates, while the Bode plot determined the impedance frequency. The CeO_2-coated mild steel plate demonstrated significantly enhanced corrosion resistance under all tested conditions, achieving a maximum corrosion inhibition efficiency of 85% in a 3.5% NaCl medium compared to uncoated MS plates.

Keywords: Bode plot, CeO_2 nanoparticle, Corrosion inhibition, Green synthesis, Nelumbo nucifera, Nyquist plot, Tafel plot

Introduction

Corrosion has been a significant issue that humanity has sought to understand and mitigate since the advent of metallic tools and structures. Damage caused by corrosion in metallic components results in substantial economic losses. These losses have contributed to numerous accidents involving airplanes, trains, ships, pipelines, and bridges, leading to countless fatalities[1]. Enhancing the use of metal oxide nanoparticles, which exhibit superior corrosion resistance, cathodic protection, and cost-effectiveness, is essential for extending the lifespan of metallic materials and addressing corrosion-related challenges. Intelligent materials that accumulate chromium ions and release them at corrosion sites during electrolyte exposure can inhibit redox processes and mitigate corrosion[2]. These materials, commonly known as chromate conversion layers, are widely employed in aeronautics and ship engines to prevent corrosion in metallic alloys. However, using chromates in various applications resulted in releasing toxic chromium species into the environment, creating an urgent need for eco-friendly alternatives[3].

Aluminum alloy AA2024 is extensively used in the aerospace sector due to its ideal weight, strength, and resistance to corrosion, achieved through the formation of a natural, inert oxide layer. However, its susceptibility to localized pitting corrosion, caused by intermetallic inclusions, can progress to exfoliation corrosion, jeopardizing the alloy's structural integrity. Nanotechnology, characterized by its rapid growth and effectiveness, has revolutionized material properties at the nanoscale, significantly enhancing physical, chemical, optical, and mechanical attributes[4]. Nanomaterials, with their high surface-to-volume ratio, wide bandgap, and superior properties, find applications in photocatalysis, supercapacitors, antibacterial treatments, corrosion resistance, cancer therapy, and solar cells. Cerium salts, a class of inorganic inhibitors, have been identified as providing active sites for corrosion inhibition without toxicity concerns[5]. Cerium oxide (CeO_2), a widely recognized rare earth oxide, demonstrates excellent corrosion resistance. CeO_2 compounds incorporated into sol-gel organic-inorganic hybrid coatings offer cathodic protection through cerium ions (Ce^{3+} and Ce^{4+}).

During oxygen reduction, hydroxide ions (OH^-) are released, forming hydroxides and insoluble cerium oxides that repair corrosion-damaged areas and prevent further redox reactions. Despite the advantages of cerium salts in coatings, limited studies have explored the inhibitory effects of CeO_2 nanoparticles (NPs). The favourable corrosion resistance of CeO_2 NPs is attributed to the diffusion of cerium cations to the metal surface, their release from nanoparticles and their re-precipitation at corrosion sites[6]. The Gibbs-Thomson effect, which enhances solubility due to the nanometer-scale particle size, facilitates the release of cerium cations. CeO_2 also reduces oxygen levels in active zones and improves coating adhesion to metallic substrates, enhancing corrosion resistance.

CeO_2 NPs were synthesized through a green, sonication-assisted method using *Nelumbo nucifera* (lotus) leaf extract as a reducing and capping agent. *N. nucifera*, the national flower of India and Vietnam, is commonly found in ponds and water gardens. It belongs to the family *Nelumbonaceae* and the order *Proteales*. The leaves contain phytochemical compounds such as alkaloids, flavonoids, phenols, and saponins. Historically, various parts of the plant have been used to treat diarrhea, tissue inflammation, aging-related ailments, diabetes, obesity, and bleeding disorders[7]. The peltate leaves of *N. nucifera*, with their water-repellent properties, have been a model for self-cleaning surface research due to their waxy polar coating and rough texture, which enable water to form droplets and roll off easily. This has spurred interest in naturally derived corrosion inhibitors, such as plant extracts, as they are cost-effective, eco-friendly, renewable, and biodegradable compared to synthetic chemical inhibitors[8].

Mild steel (MS), widely used in automotive, furniture, fencing, and structural construction industries, is a cost-effective material with good mechanical properties. However, its high carbon content makes it susceptible to corrosion, particularly in marine environments and industrial applications exposed to corrosive substances such as NaCl, KOH, and HCl. Corrosion occurs when electrolytes facilitate the oxidation of the anode metal, leading to the loss of electrons and the formation of rust. Electrolytes such as NaCl, KOH, and HCl accelerate this process by providing ions that sustain the redox reactions. One of the simplest ways to mitigate corrosion is through barrier coatings, such as paint or plastic. However, these methods offer only temporary protection[9].

In contrast, nanotechnology provides a long-term solution by leveraging the unique properties of NPs. Yang et al. studied the effects of additives and post-treatments on PEO coatings for magnesium and titanium. Adding SiO_2 particles significantly improved mechanical and corrosion properties of the coating, with EIS measurements showing increased impedance modulus, indicating enhanced corrosion resistance. The NiO NPs using *Delonixelata* leaf extract via ultrasonic-assisted green synthesis. NiO NP-coated plates showed significantly reduced corrosion rates in 3.5% NaCl, 6 M KOH, 1 M HCl, and 1 M H_2SO_4, with the best results in H_2SO_4 which demonstrates biosynthesized NiO NPs as eco-friendly, effective corrosion inhibitors for Zn and Mg alloys. The withered flower petals (rose and lotus) as natural antioxidants to synthesize MnO_2 resulted in improved corrosion resistance of MS, with inhibition efficiencies of 72.63% for lotus-derived and 51.50% for rose-derived MnO_2. The eco-friendly, cost-effective approach offers promise for industrial applications. This study used CeO_2 NPs synthesized using the water-repellent and self-cleaning *N. nucifera* leaf extract to coat mild steel plates. Corrosion studies were conducted on the coated plates under three different electrolytes (NaCl, HCl, and KOH), and the influence of CeO_2 NPs on the corrosion resistance of MS plates is discussed in detail[6-9].

Experimental Section

Materials required

Cerium nitrate hexahydrate ($Ce(NO_3)_3.6H_2O$, *N. nucifera* leaves, double distilled water, ethanol, n-methyl pyrrolidine, polyvinyledene fluoride (PVDF), MS plate, sodium chloride (NaCl), HCl and potassium hydroxide (KOH) were used. Emery paper ranging from grades 60 to 1200 was used to prepare the surface of the MS plate. They were rinsed in double-distilled water, and then acetone was applied afterward. Then, it is dried in sunlight before its immersion in the electrolyte. No further purification was done to any of the chemicals since they were all obtained from Merck.

Preparation of *N. nucifera* leaf extract

The leaves of *N. nucifera* are collected from the pond, then washed and dried in the shade to avoid the loss of phytochemicals. After that, a mixer grinder set to 20,000 revolutions per minute was used to grind the dried leaves into a powder. To make an extract,

5 g of the obtained powder was mixed in 100 mL of hot double distilled water and stirred at 60°C for an hour and without heat for 24 h for the maximum extraction of phytochemicals from the leaf extract. The phytochemicals show a significant role in nanoparticle formation, which reduces and caps over the surface of the CeO_2 NPs. After stirring, the solution was filtered using a Whatman filter paper for further use.

Synthesis of CeO_2 NPs

Initially, 0.1M of cerium nitrate ($Ce(NO_3)_3.6H_2O$ salt was dissolved in 100 mL of the above-prepared leaf extract and stirred until a homologous mixture was formed. The solution was stirred overnight at room temperature to attain the homologous solution. When the homologous mixture was obtained, the solution was kept aside for 24 h for aging. Aging is a process of the formation of NPs where nucleation followed by growth occurs, and it has size, shape, and morphology modifications. After aging, the mixture was exposed to a sonication process for 60 min, in which a uniform distribution of particles occurs and reduced the chance of agglomeration. The mixture was then washed by centrifuge with distilled water followed by ethanol and distilled water to get Cerium oxide NPs without impurities. The solution was dried using a hot air oven at 60°C for 8 h to vapourise water. Then, the dried powder was ground using a mortar and pestle to obtain a fine powder. The powder was then annealed by a muffle furnace at 400°C for 3 h, making the NP highly crystalline and eliminating volatile materials. Then, the obtained NPs are stored in a container for further use. The whole process is shown in Fig.1.

Coating over MS plate

The doctor's blade method was used to develop a nanostructured coating over the surface of the MS plate. Initially, the MS plate was polished using emery paper to remove rust and dust that settled over the surface. The MS plate was polished, cleaned with distilled water, then acetone and distilled water, and allowed to dry at room temperature. Then, the prepared CeO_2 NPs are mixed with PVDF and n-methyl pyrrolidone at 80:15:5 using a mortar and pestle. Here, PVDF acts as a binder at the surface of the plate, and n methyl pyrrolidine acts as a solvent. When the mixture is formed, it is coated over the surface of the MS plate at an area of 1 cm^2 using a doctor's blade. The process is repeated several times until the uniform coating is attained. The MS plate is dried after coating in a hot air oven for one hour at 60°C to eliminate water. Finally, the coated MS plates were used for the corrosion analysis in various electrolytes, such as 3.5% NaCl, 1 M HCl, and 1M KOH solutions.

Electrochemical setup

A three-cell setup was performed using various electrolytes to estimate the corrosion characteristics of the coated MS plate. In these three-cell setups, the working electrode was an MS plate, the counter electrode was a platinum electrode, and the reference electrode was a saturated calomel. Electrochemical corrosion studies were carried out (until obtaining the

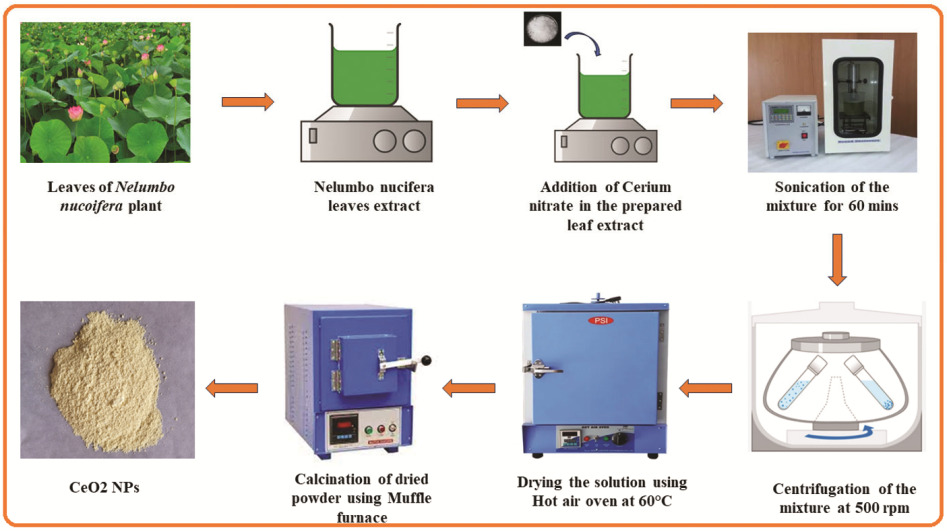

Fig. 1 — Schematic diagram for cerium oxide synthesis

concurrent value) for the MS plate (before and after coating with CeO_2 NPs) in different electrolytes (3.5% NaCl, 1M HCl, and 1M KOH) using Autolab PGSTAT302N equipment (The Netherlands). A potential window of 1.8 to 1 V at a scan rate of 5 mV s^{-1} was used for the corrosion investigations. According to extrapolated data from the cathodic and anodic portions of the potentiodynamic polarization test or the Tafel plot were calculated. All electrochemical measurements were carried out three times to ensure the findings could be replicated.

Materials characterization

The XRD pattern of CeO_2 NPs was determined using a powder X-ray diffractometer (PANalytical, Almelo, the Netherlands) with CuKα at 40 kV, 30 kV, and 30 mA. Using KBR as the active medium, an FTIR spectrophotometer (Perkin Elmer, USA) was used to record the spectra of the CeO_2 NPs. The standard particle size distribution was studied using a particle size analyzer (Sympatec, Germany) that uses the DLS technique and a laser beam with a wavelength of 633 nm. UV-visible spectrophotometer (Cary 8454; Agilent) was used to analyze the absorption bands of the produced CeO_2 NPs. The morphology and structure of the sample were examined using a HRTEM with a 200 kV (JEOL; Japan). The surface of the CeO_2 NPs was examined using SIGMA HV FESEM. The photoluminescence spectroscopy (Cary Eclipse, Agilent Technologies) was taken to examine the luminescence properties of the prepared CeO_2 NPs. The CeO_2-coated MS plates are submerged for 24 h in different electrolytes to investigate the corrosion-prevention capabilities of the coatings. An electrochemical workstation (PGSTAT302N; The Netherlands) equipped with three electrodes was used to study the electrochemical corrosion behaviour of CeO_2-coated and pure MS plates.

Results and Discussion

Fig. 2 displays the XRD peaks of CeO_2 nanoparticles located at an angle (2θ) of 28.45, 33.12, 47.55, 56.33, 58.98, 69.06, 763.45, and 78.95, which corresponds to the miller indices of (111), (200), (220), (311), (222), (400), (331), and (420) planes of CeO_2, respectively. The typical diffraction peaks demonstrate that the face center cubic phase of CeO_2 NPs is consistent with the JCPDS card number 34-0394. The average crystallite size of CeO_2 was found to be 9.8 nm using Debye-Scherrer equation[10] (Eq. 1) as given below.

$$D = \frac{K\lambda}{\beta\cos\theta} \quad \ldots (1)$$

Where, D represents the typical crystallite size, K is Scherrer constant (0.9), 1.541 indicates the wavelength of Cu Kα, β is full width half maximum (FWHM) of the diffraction peak and θ is the angle of diffraction. The lattice constant 'a' of CeO_2 was calculated using the following equation[11],

$$d = a/(h^2+k^2+l^2)^{1/2} \quad \ldots (2)$$

Where, the miller index of the diffracted plane is denoted by (hkl). The number of dislocation lines per unit crystal volume is called the dislocation density and may be computed using the Williamson–Smallman relation, which can also be estimated[11].

$$\text{Dislocation density} = 1/D^2 \quad \ldots (3)$$

The degree to which the crystalline lattice has been distorted might be called the macrostrain. The widening of the XRD lines may be influenced by microscopic strain in the crystal lattice. It is possible to figure out by using the formula[12],

$$\varepsilon = \frac{\beta}{4\tan\theta} \quad \ldots (4)$$

Where,ε is the microstrain in radians, which is the ratio of peak width to peak position, β is the line broadening at FWHM in radians, and θ is the Braggs angle in degrees, half the 2θ. The values found using XRD, such as microstrain, lattice constant, and crystal size, are shown in Table 1.

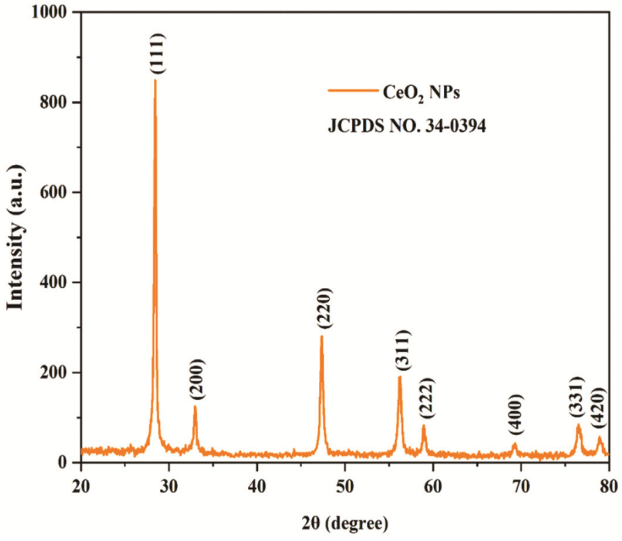

Fig. 2 — X-ray diffractogram of synthesised CeO_2 NPs

Table 1 — Structural parameters from Rietveld refinement profiles of the synthesized CeO_2

Crystal structure	Cubic
Space group	Fm3m
Crystal size	9.8 nm
Lattice parameter	5.178 (a=b=c)
Volume	138.38 Å^3
Lattice strain	0.0028
Micro strain	0.31 %
Dislocation density	1.04 ×10^{-3} (nm)$^{-2}$
R_p	10.5
R_{wp}	13.1
R_{exp}	8.54
Chi^2	1.75

Rietveld refinement

The Rietveld refinement for the *N. nucifera*-prepared CeO_2 NPs is given in Fig. 3. This improvement is made to highlight the discrepancy between the predicted and actual XRD data patterns. Full proof analytical software uses the pseudo-Voigt profile function to refine the Rietveld refinement. Every one of the samples was improved by taking into account the space group Fm3m and its cubic structure. The refined parameters and the R factors achieved are depicted in Table 1. 5.178 is the value obtained by refining the lattice constant of CeO_2 NPs. There is an immediate match between the improved lattice parameters and the JCPDS card no. 34-3964.

Functional group analysis

The result of FTIR analysis is shown in Fig. 4. The peak at 471 cm^{-1} is attributed to the stretching vibrations of Ce–O bond. The strong absorption bands at 3436 cm^{-1} are assigned to the -OH stretching vibrations of the absorbed water. The dual peak at 2864 and 2933 cm^{-1} indicates the symmetrical and asymmetrical stretching of the $=CH_2$ and $-CH_3$ groups, denoting the presence of the alkane group[12]. Also, the weak peak at 604 cm^{-1} is assigned to the CeO_2 presence. The C=O stretching of amide-I bands of peptide linkage is shown by the emergence of a peak at around 1635 cm^{-1}.

The band at 962 cm^{-1} could be ascribed to the vibrational stretching mode of H_2O. The outward bending vibration of the C-H group of the dispersed benzene ring is thought to be responsible for the absorption peak at 798 cm^{-1}. An intense peak at 1087 cm^{-1} can be assigned to the C-O stretching vibration of an alkaloid species[13].

Particle size analysis

As illustrated in Fig. 5, the mean particle size of the synthesized CeO_2 NPs was determined using the DLS

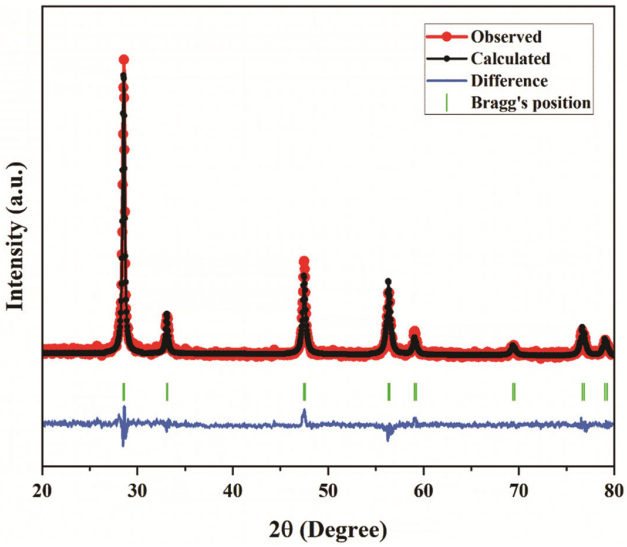

Fig. 3 — Rietveld refinement of synthesised CeO_2 NPs

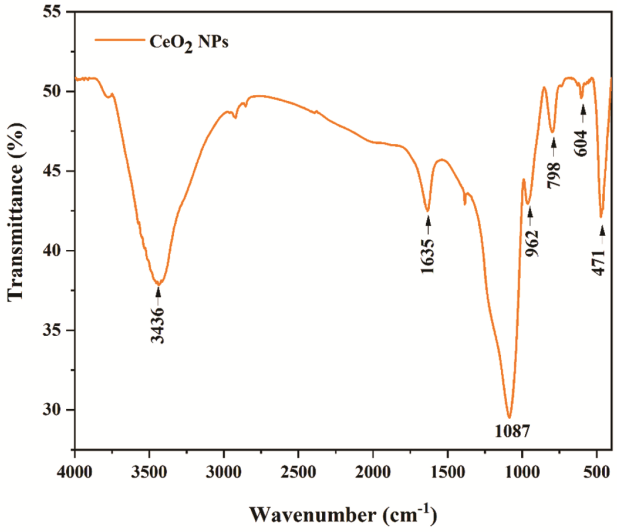

Fig. 4 — FTIR spectrum for synthesised CeO_2 NPs

method. The average particle size (d_{50}) was found to be 18.48 nm. The phytochemical compounds in *N. nucifera* leaves contribute to the reduction in particle size. The particle size is consistent with the crystalline size obtained from XRD analysis and the morphology observed in TEM images. The d_{10} and d_{90} values were determined to be 3 nm and 89 nm, respectively, indicating that most of the synthesized particles fall within the nanometer range. The particle size is crucial in the material's corrosion resistance efficiency. Smaller particle sizes offer a higher surface area, which can enhance reactivity. While this increased reactivity may lead to susceptibility to specific forms of corrosion, it can also promote the

formation of protective layers under certain conditions, thereby improving corrosion resistance.

Morphological analysis

The FE-SEM and the HR-TEM are used to conduct the morphological investigation of the CeO_2 NPs. The SEM images of the produced CeO_2 NPs are shown in Fig. 6. The SEM analysis implies that the synthesized NPs of CeO_2 have a foam shape, which may be attributed to the aggregation condition of the CeO_2 NPs with one another. This aggregation indicates that the synthesized cerium oxide NPs have a high surface charge. The elemental makeup of the produced CeO_2 NPs in the EDX spectrum is shown in Fig. 6 (d). According to the results of the EDX examination, the only elements present are cerium and oxygen, with respective weight percentages of 83.26 and 16.47. The EDX spectrum makes it abundantly evident the formation of pure cerium oxide without any additional elements or impurities.

Fig. 7 shows the transmission electron microscope (TEM) images of CeO_2 nanoparticles. The particles were found to be nearly spherical and highly agglomerated. The average particle size is found to be 18 nm. The prominent discrete rings seen in Figure 6 (d) suggest that the CeO_2 NPs are polycrystalline in nature[14], which is consistent with the results of the XRD analysis. The approach of dynamic light scattering is also compatible with the size of the particles, as was previously stated.

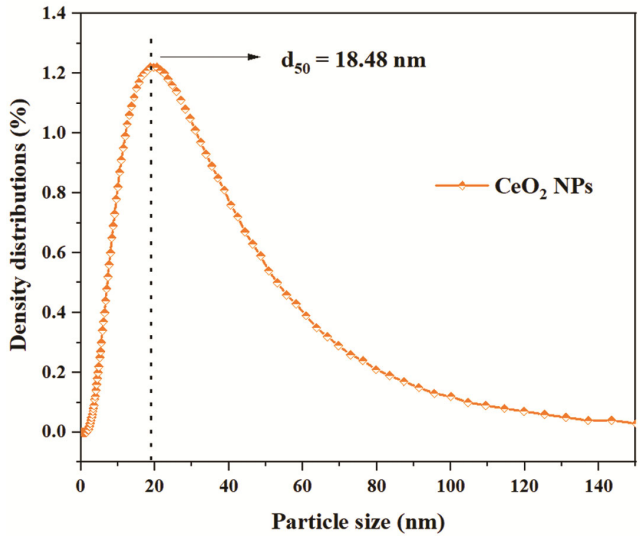

Fig. 5 — Particle size analysis of synthesised CeO_2 NPs

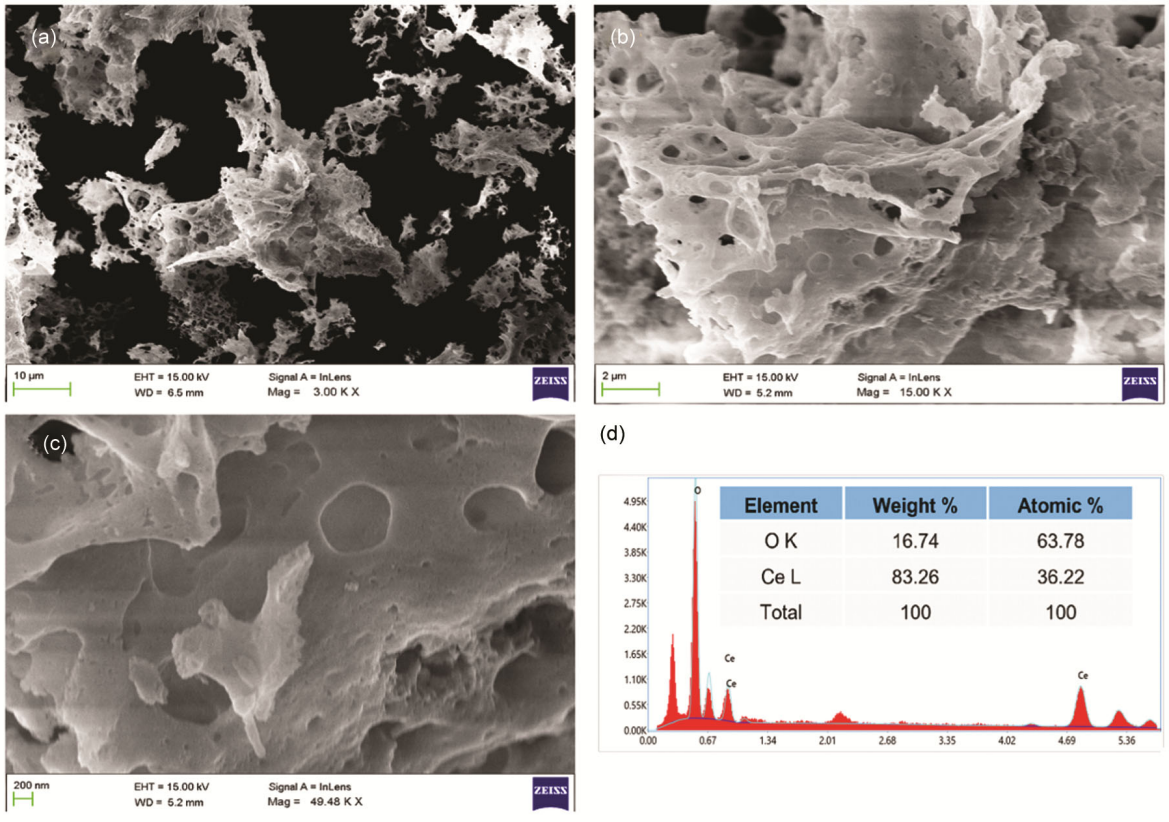

Fig. 6 — SEM images of synthesised CeO_2 NPs

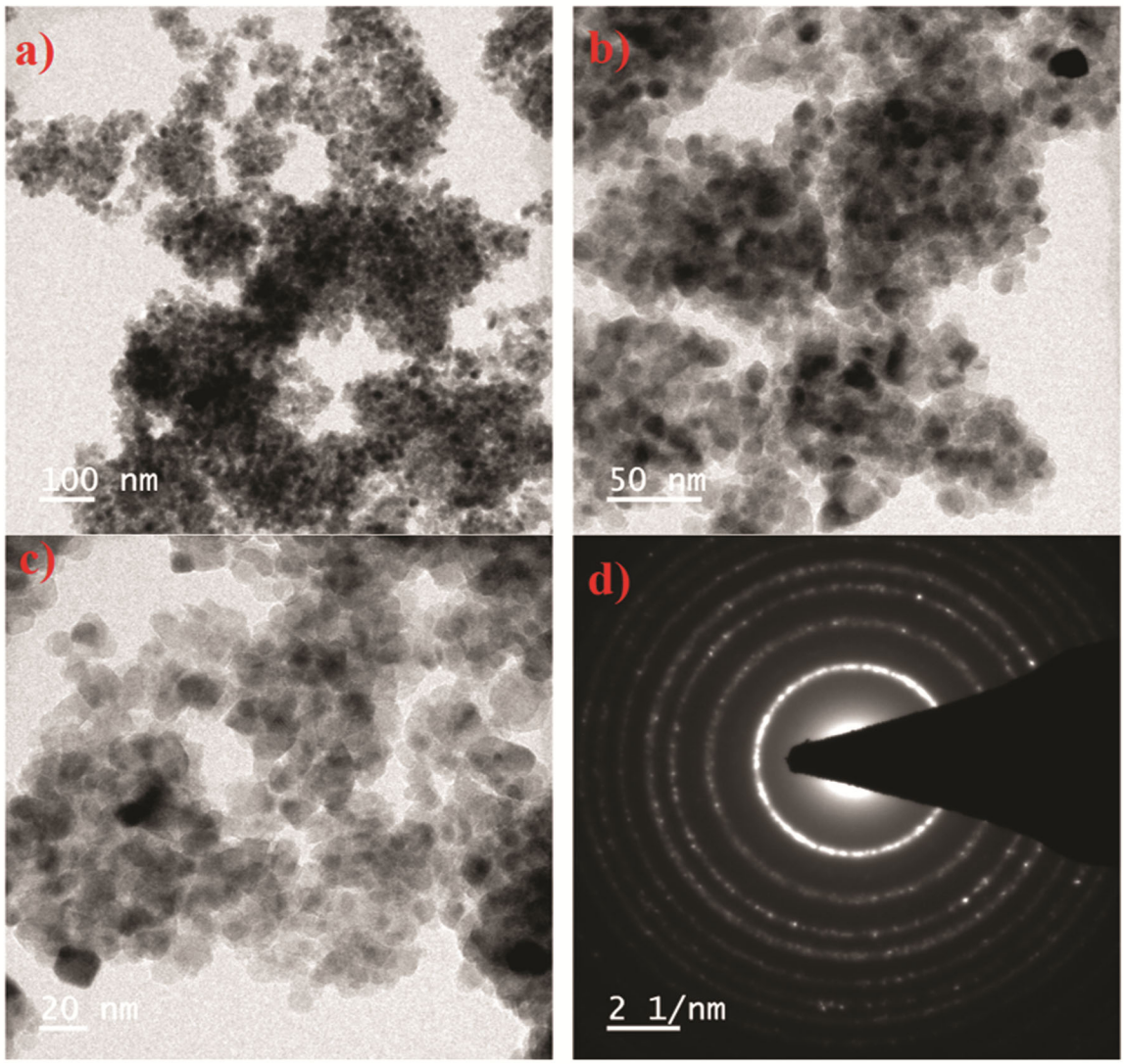

Fig. 7 — TEM analysis of synthesised CeO_2 NPs

UV-visible absorption analysis of CeO_2 NPs

The UV-visible absorption spectrum of CeO_2 NPs, is shown in Fig. 8. The typical absorption peak of Ce^{3+} and Ce^{4+} of CeO_2 NPs was reported to be at 208 and 300 nm, which correlates to the peak of absorbance detected at these wavelengths. Ions with the charge states of Ce^{3+} and Ce^{4+} may be seen in the spectrum. These forms of ions presence have a significant role in corrosion resistance[15].

The direct bandgap for CeO_2 NPs was determined by the Tauc's plot from the spectrum observed using Diffuse reflectance spectroscopy (DRS). The absorption efficiency is correlated to incident photon energy using the formula[16],

$$\alpha(\upsilon)h = K(h\upsilon - E_g)^n \quad \ldots (5)$$

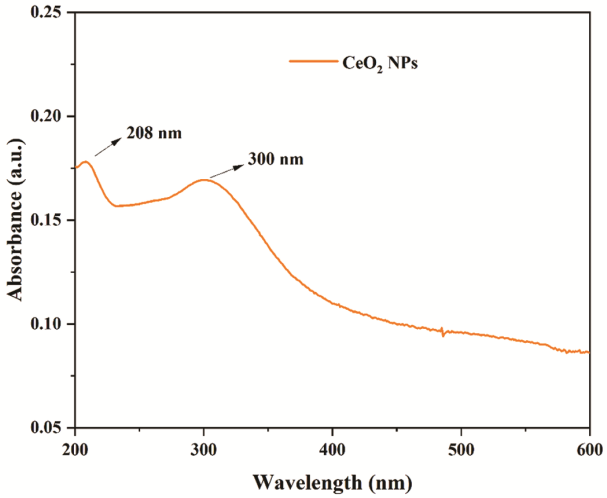

Fig. 8 — UV visible absorption spectrum of synthesised CeO_2 NPs

The calculated band gap of the prepared CeO_2 was 2.97 eV, as shown in Fig. 9.

Luminescence property

Using photoluminescence spectroscopy, it is possible to ascertain the fluorescence characteristics of the CeO_2 NPs. The luminescence characteristic of CeO_2 NPs was measured at room temperature using an excitation wavelength of 300 nm, as seen in Fig. 10. A luminous band was observed at 600 nm and is connected to the charge-transfer transition. Because trivalent cerium does not emit light, we may deduce that the nanocrystal has a relatively low oxygen vacancy.

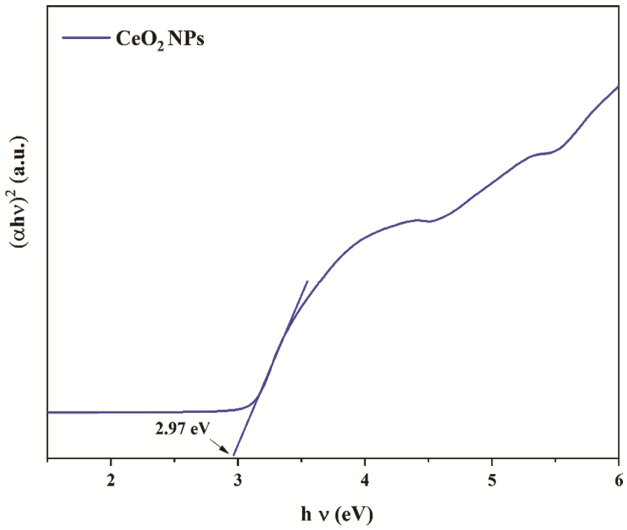

Fig. 9 — Tauc plot for calculation of bandgap of synthesised CeO_2 NPs

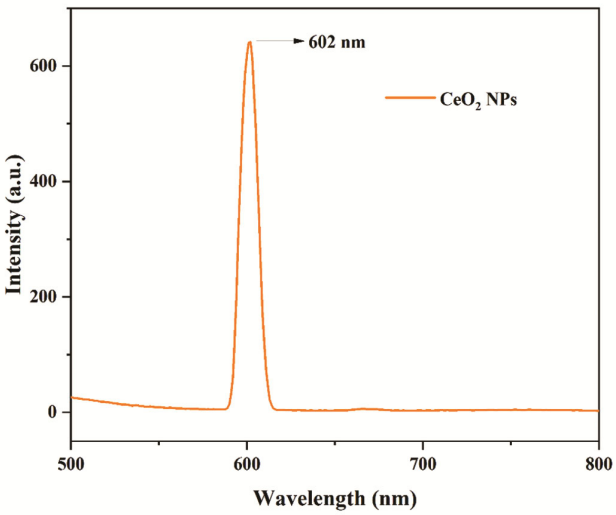

Fig. 10 — PL spectrum for synthesised CeO_2 NPs

Impedance studies

Electrochemical impedance spectra, also known as a Nyquist plot, are depicted in Fig. 11 (a, b & c) for MS and CeO_2-coated MS plates for 1M HCl, 1M KOH, and 3.5% NaCl solutions. At low frequencies, the Nyquist plot showed the formation of a half circle, which may have a linear relationship to the resistance of charge transfer reaction. The radius of the semicircles shown by each sample in Fig. 11 varies noticeably depending on whether the plates are coated or uncoated. The electrical phenomenon loops were noted in all examined electrolytes. The coated samples displayed higher barrier properties in resistance to the electrochemical corrosion process, as shown by the CeO_2-coated MS plate's electrical phenomena values being higher than those of the untreated plates. It was great to see that in 1M HCl, 1M KOH, and 3.5% NaCl, the arc and Rp (Rct) values of CeO_2-coated MS metal surfaces were much more significant than those of uncoated MS plates.CeO_2, which creates a safe coating layer over the MS plate surface, controls the free discharge of electrons or oxidation from the MS plate. This layer is created when the MS plate is submerged in aqueous electrolytes. The CeO_2-coated MS plates with a high charge transfer resistance (Rct) value exhibit superior corrosion resistance on the metal surface as compared to bare plates[17]. These electrochemical impedance spectra for CeO_2-coated MS plates with three different electrolytes reveal that the produced CeO_2 NPs have a high resistance level to electrochemical corrosion. The various impedance parameters determined in electrochemical impedance studies for uncoated MS plate and CeO_2-coated MS plate in different aqueous mediums are listed in Table 2.

Corrosion studies

Fig. 12 shows the Tafel plots, also known as the potentiodynamic polarization curves, for the MS plate and CeO_2-coated MS plate in 1M HCl, 1M KOH, and 3.5% NaCl. The electrochemical corrosion parameters, which are shown in Table 3, were determined using the Tafel plot. The electrochemical corrosion inhibition characteristics of MS plate are addressed in an electrolyte-by-electrolyte manner for ease of comprehension; electrochemical corrosion inhibition behaviour of MS plate are discussed electrolyte-wise. In an electrolyte solution containing 1M of HCl, the corrosion potential (E_{corr}) of CeO_2-coated MS plates is more favourable than that of pure MS plates. This is the case when

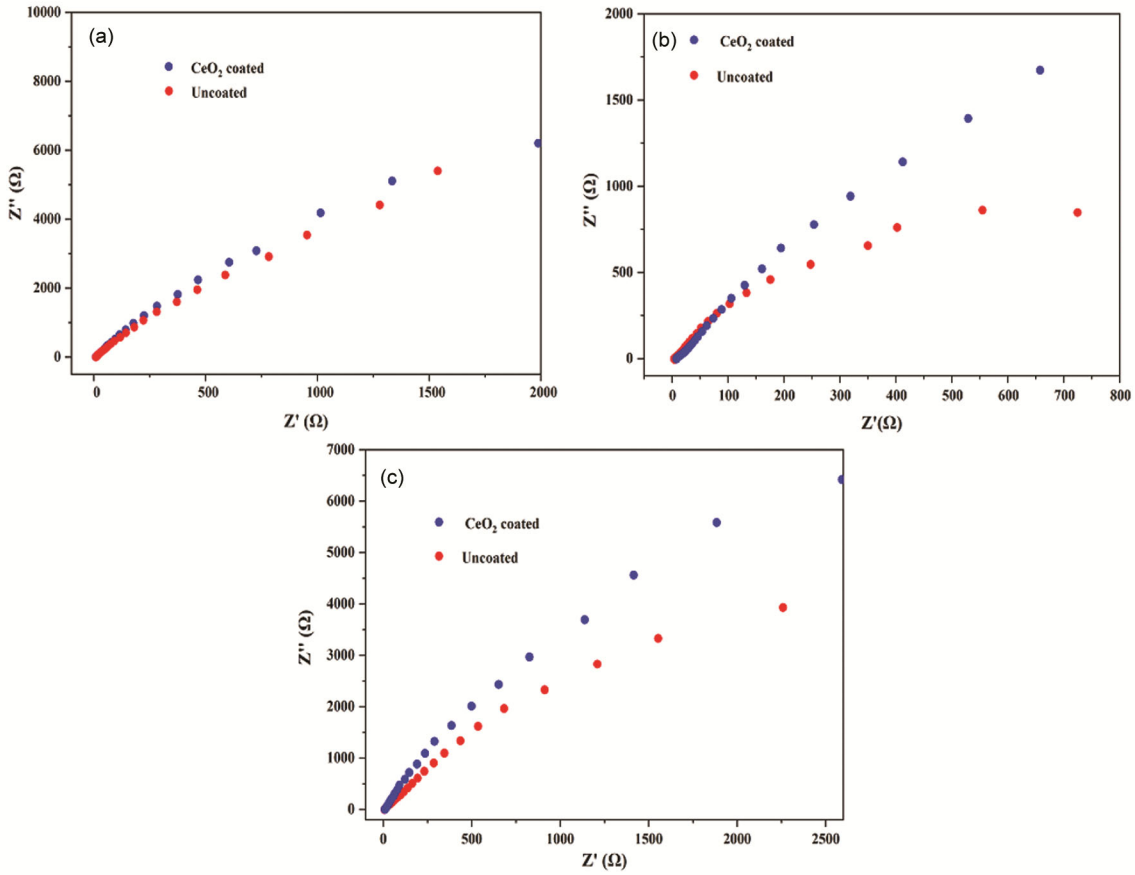

Fig.11 — Electrochemical Impedance for CeO_2 coated and uncoated MS plates in (a) HCl, (b) KOH and (c) NaCl media

Table 2 — Impedance parameters in various aqueous electrolytes

Medium	Substrate	R_s. R (Ω)	R_p. R (Ω)	CPE.N (μF)	CPE.Y0 (μF)
1M HCl	MS	4.348	19540	0.99418	8.1451 E-05
	MS-CeO_2	8.2519	36613	0.9964	4.347 E-05
1M KOH	MS	7.7681	13233	0.99803	0.00012027
	MS-CeO_2	8.435	65283	0.9981	2.4379 E-05
3.5% NaCl	MS	9.0697	44060	0.99791	3.2441 E-05
	MS-CeO_2	$9._2$498	49536	0.99785	3.1073 E-06

comparing the two types of plates. The addition of inhibitor CeO_2 causes the corrosion potential of MS plates, from -1.0163 V to -0.94193 V. This results in a decrease in the corrosion current of CeO_2-coated MS plates. At a given corrosion rate, the CeO_2 coating reduces the corrosion current (I_{corr}), the primary factor determining the corrosion rate. The corrosion rate of pure MS plate is 1.2867 mm/year, whereas the corrosion rate decreased for CeO_2 coated MS plate is about 0.4681 mm/year, which reduces approximately 65.46% of corrosion. The polarization resistance of pure MS plate and CeO_2-coated MS plate is 202.2 Ω and 445.43 Ω, which suggests better corrosion inhibition. Meanwhile, the corrosion potential of the pure MS plate and CeO_2-coated MS plate were determined to be -0.9708 V and -0.65674, respectively, in the 1M KOH solution. These values were found to be negative. The corrosion potential values of CeO_2 coated MS plate significantly decrease compared to those of the pure MS plate. The uncoated MS plate showed a corrosion rate of 1.8213 mm/year; for CeO_2 coated, the corrosion rate is 0.47157 mm/year, decreasing the corrosion by 74.11%.

The polarization resistance for uncoated and CeO_2-coated MS plates shifts from 87.928 to 470.64 Ω, improving corrosion inhibition. The findings of an electrolytic solution containing 3.5% NaCl revealed

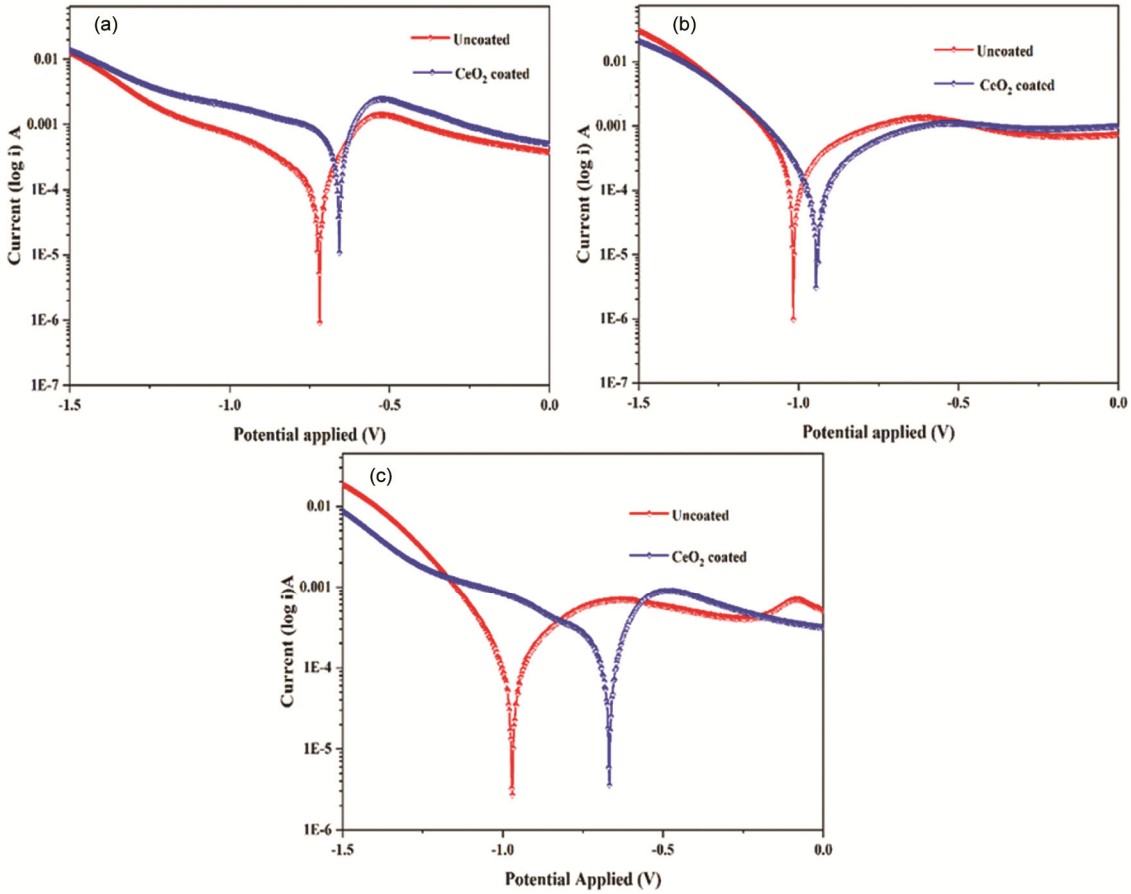

Fig.12 — Electrochemical corrosion analysis for CeO_2 coated and uncoated MS plates in (a) HCl, (b) KOH and (c) NaCl

Table 3 — Tafel polarization parameters

Medium	Substrate	E_{corr} (V)	I_{corr} (A)	Polarization Resistance (Ω)	Corrosion rate (mm/year)	Efficiency (%)
1M HCl	MS	-1.0163	0.00010918	202.2	1.2687	
	MS-CeO_2	-0.94193	4.0292E-05	445.43	0.4681	65.46
1M KOH	MS	-0.9708	0.00015674	87.928	1.8213	
	MS-CeO_2	-0.65674	4.0583E-05	470.64	0.47157	74.11
3.5% NaCl	MS	-0.72117	3.7837E-05	335.78	2.13966	
	MS-CeO_2	-0.66788	0.6183E-05	416.28	0.30424	85.78

that CeO_2-coated MS plates were polarized anodically. This indicates that these plates were more able to suppress corrosion than pure MS plates. The MS plate with a CeO_2 coating had a considerably greater corrosion potential, or E_{corr}, than the untreated MS plate. This shows that the corrosion rate of the CeO_2-coated MS plates is lower (0.30424 mm/year) than the corrosion rate of the naked MS plates (2.13966 mm/year), which improves the corrosion inhibition rate by about 85.78 % and the polarisation resistance of uncoated and CeO_2 coated MS plate is 335.75 and 416.28 Ω, respectively.

As previously indicated, the results prove that a surface coating consisting of a thin layer of CeO_2 NPs on an MS plate is essential for obtaining a low corrosion rate and a significant resistance to electrochemical corrosion. A thorough review of the relative efficiency of nanomaterial coatings on metal surfaces in terms of improved corrosion protection behaviour is given in Table 3. The table shows that CeO_2 is a promising material for improving corrosion resistance in the MS plate. The CeO_2 NPs show high-efficiency corrosion inhibition in a seawater medium, about 85%, which can be used as

an anti-corrosive agent for mild steels in ship machinery. When applied to the surface of metals, the CeO_2 NPS may serve as a barrier to protect against corrosive elements, including oxygen and moisture. The CeO_2 can act as a cathodic protection agent by performing as a sacrificial anode with high anodic polarization. CeO_2 NPs have intrinsic antioxidant properties, effectively scavenging oxygen radicals and preventing oxidative corrosion[17].

The phytochemicals in the *N. nucifera* leaves make the CeO_2 NPs with corrosion inhibition properties, reducing the particle size and releasing Ce^{3+} and Ce^{4+} ions, which are responsible for improved corrosion inhibition properties. Hence, it is concluded that CeO_2 nanoparticles are used as a corrosion inhibitor in various aqueous electrolytes. The Nyquist plots have the inherent constraint of not revealing the specific frequencies at which the impedance values are measured. Plotting Bode diagrams, which show how the system behaves regarding frequency-specific impedance, is one way to get around this issue. Fig. 13 shows that only one time constant could be

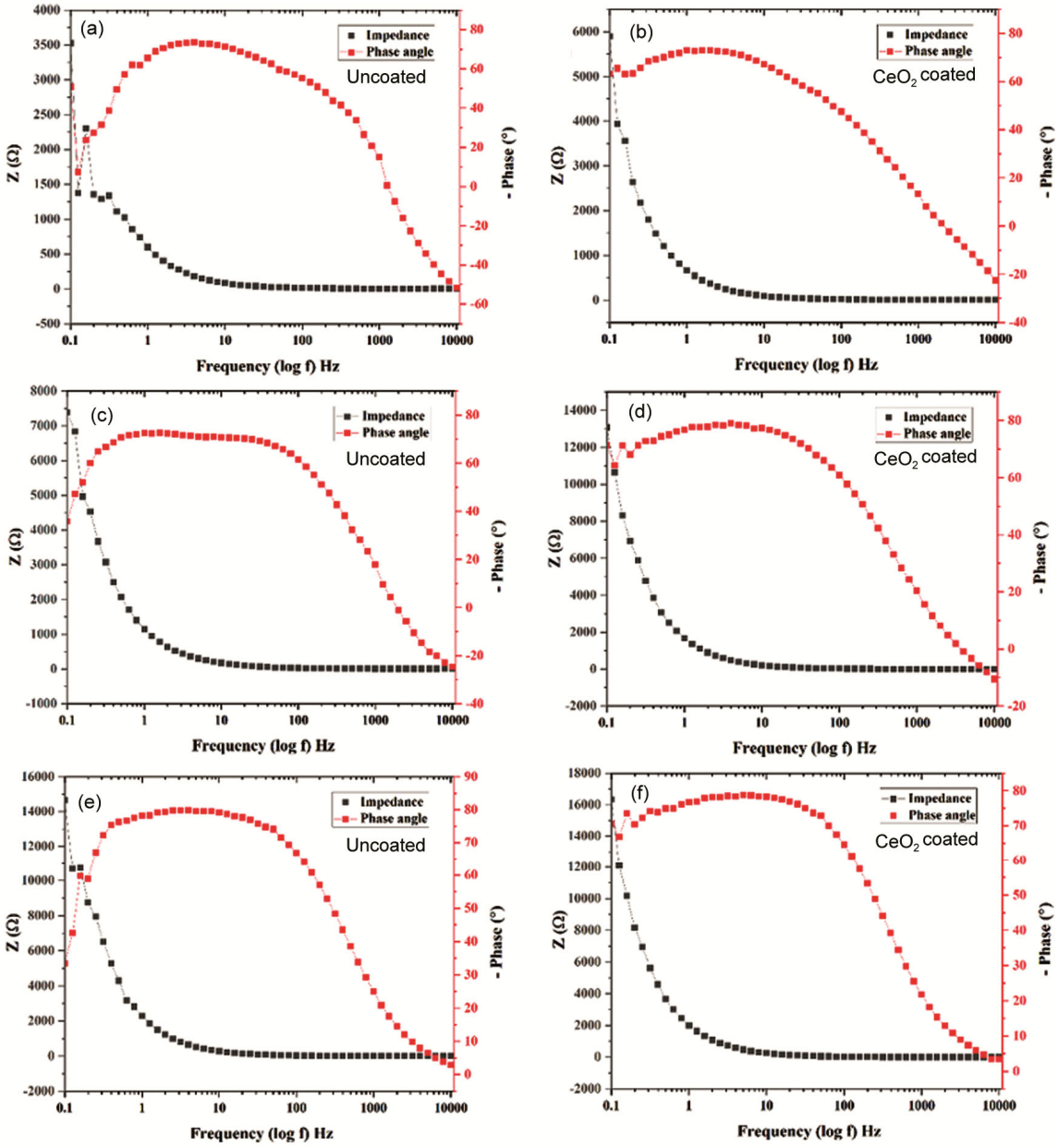

Fig.13 — Bode plot for uncoated and CeO_2coated MS plate in (a and b) 1M HCl, (c and d) 1M KOH, (e and f) 3.5% NaCl

seen and that the phase angle became more prominent as the concentration of RS rose. This indicates that the surface homogeneity is becoming less consistent. Consequently, the protective efficacy improves when there is a higher concentration of RS.

Conclusion

The sonication-assisted green synthesis approach by utilizing *Nelumbo nucifera* leaf extract as a reducing and stabilizing agent effectively produced CeO_2 NPs. The ultrasonic waves significantly contributed in formation of highly crystalline and pure CeO_2 NPs. Positive results from absorption and PL analyses confirmed the material's excellent optical quality. The synthesized CeO_2 NPs exhibited nanoscale particle sizes, with an average diameter of approximately 18 nm, which can be attributed to the combined effects of ultrasonic vibrations and the bioactive components of *N. nucifera* leaf extract. Morphological studies revealed that the CeO_2 NPs possessed nearly spherical shape, consistent with the results obtained from particle size analysis. In corrosion studies, CeO_2-coated MS plates demonstrated superior corrosion resistance in 3.5% NaCl solution compared to other tested electrolyte media. Specifically, the corrosion resistance improved by 85.78% in the seawater medium, while corrosion inhibition efficiencies of 65.46% and 74.11% were observed in 1M HCl and 1M KOH solutions, respectively. These findings highlight the potential of CeO_2 NPs synthesized using *N. nucifera* leaf extract as a promising material for enhancing the corrosion inhibition properties of MS plates.

References

1 Chai W S, Cheun J Y, Kumar P S, Mubashir M, Majeed Z, Banat F, Ho S H & Show P L, A review on conventional and novel materials towards heavy metal adsorption in wastewater treatment application, *J Clean Prod*, 296 (2021) 126589.

2 Xie C, Zhang P, Xue M, Yin Z, Luo Y, Hong Z, Li W & Zhang Z, Long-lasting anti-corrosion of superhydrophobic coating by synergistic modification of graphene oxide with polydopamine and cerium oxide, *Constr Build Mater*, 418 (2024) 135283.

3 Hao L, Jiang Z, Fang Y, Zhou Y, Fu B & Lin L, Understanding the role of oxygen vacancy on corrosion resistance of coating containing cerium oxide nanoparticles doped with cobalt as highly effective corrosion inhibitors, *Appl Surf Sci*, 626 (2023) 157300.

4 Hosseini M, Fotouhi L, Ehsani A & Naseri M, Enhancement of corrosion resistance of polypyrrole using metal oxide nanoparticles: Potentiodynamic and electrochemical impedance spectroscopy study, *J Colloid Interf Sci*, 505 (2017) 213.

5 Mendez J A C, Vong Y M & José-de-Jesús P B, Cerium and other rare earth salts as corrosion inhibitors-A review, *Prot Met Phys Chem Surf*, 58 (2022) 801.

6 Kaygusuz H & Erim F B, Biopolymer-assisted green synthesis of functional cerium oxide nanoparticles, *Chem Papers*, 74 (2020) 2357.

7 Kumar S, Ojha A K, Patrice D, Yadav B S & Materny A, One-step in situ synthesis of CeO_2 nanoparticles grown on reduced graphene oxide as an excellent fluorescent and photocatalyst material under sunlight irradiation, *Phys Chem Chem Phys*, 18 (2016) 11157.

8 Nawaz M, Shakoor R A, Kahraman R & Montemor M F, Cerium oxide loaded with Gum Arabic as an environmentally friendly anti-corrosion additive for coated steel protection, *Mater Des*, 198 (2021) 109361.

9 Meena R K, Hazardous effect of chemical wood preservatives on environmental conditions, ecological biodiversity and human being and its alternatives through different botanicals: A review, *Environ Ecol*, 40 (2022) 1137.

10 Melchers R E, Development of new applied models for steel corrosion in marine applications including shipping, *Ships Offshore Struct*, 3 (2008) 135.

11 Tungmunnithum D, Pinthong D & Hano C, Flavonoids from nelumbo nucifera gaertn a medicinal plant: Uses in traditional medicine, phytochemistry and pharmacological activities, *Medicine*, 5 (2018) 127.

12 Uddin M S, Hall C & Murphy P, Surface treatments for controlling corrosion rate of biodegradable Mg and Mg-based alloy implants, *Sci Technol Adv Mater*, 16 (2015) 053501.

13 Xia D H, Deng C M, Macdonald D, Jamali S, Mills D, Luo J L, Strebl M G, Amiri M, Jin W & Song S, Electrochemical measurements used for assessment of corrosion and protection of metallic materials in the field: A critical review, *J Mater Sci Technol*, 112 (2022) 151.

14 Dong Y, Zhang Y, Cui X J, Li M, Xie C & Pan Z, Surface-modified cerium oxide as a corrosion inhibitor to enhance the performance of epoxy coatings, *Anti-Corros Methods Mater*, 70 (2023) 149.

15 Yang Y, Yan T, Hou C, Zhang Y, Xue Z, Zhang J & Chen F, Corrosion and bacterial resistance of MAO-PA composite coating on AZ91 magnesium alloy, *J Mater Sci*, 60 (2025) 823.

16 Yepes A G, Freijedo F D, Lopez O & Doval-Gandoy J, Analysis and design of resonant current controllers for voltage-source converters by means of nyquist diagrams and sensitivity function, *IEEE Trans Ind Electron*, 58 (2011) 5231.

17 Zakeri A, Bahmani E, Aghdam A S R, Plant extracts as sustainable and green corrosion inhibitors for protection of ferrous metals in corrosive media: A mini review, *Corros Commun*, 5 (2022) 25.